A Normalized Complex LMS Based Blind I/Q Imbalance Compensator for GFDM Receivers and Its Full Second-Order Performance Analysis

Hao Cheng, *Student Member, IEEE*, Yili Xia, *Member, IEEE*, Yongming Huang, *Senior Member, IEEE*, Luxi Yang, *Member, IEEE*, and Danilo P. Mandic, *Fellow, IEEE*

***Abstract*—Generalized frequency division multiplexing (GFDM) has become one of the most important waveform candidates for air interface in 5G communications. However, like the standard orthogonal frequency division multiplexing (OFDM), its direct-conversion receivers are vulnerable to radio frequency impairments, due to their cost and size constraints. In this paper, the performance deterioration resulting from inphase/quadrature (I/Q) imbalance is first analyzed in terms of signal-to-interference plus noise ratio (SINR) for typical GFDM receivers. Next, a blind adaptive I/Q imbalance compensator based on normalized complex least mean square (NCLMS), originally designed for OFDM receivers, is extended for GFDM ones. In order to provide more physical insight into its compensation capability, a full second-order performance assessment is established, via a joint consideration of the weight error variance and its complementary variance of the proposed compensator in both the transient and steady-state stages. Apart from an accurate evaluation on its overall self-image attenuation performance, the proposed full second-order analysis is also able to quantify the individual contributions from both the I and Q channels of the compensator, an important finding missing in the literature and not possible to discover by using the standard variance analysis only. This analysis also facilitates theoretical quantifications of SINR improvements by NCLMS for GFDM receivers. Simulations on GFDM waveforms support the analysis.**

***Index Terms*—GFDM, inphase/quadrature (I/Q) imbalance, improperness, NCLMS, full second-order performance analysis, SINR analysis, image rejection ratio (IRR) analysis.**

I. Introduction

GENERALIZED frequency-division multiplexing (GFDM), which is a block based filtered multi-carrier modulation scheme, has become one of the most important waveform candidates for air interface in 5G communications [1], [2]. By carefully designing the underlying circular filters with windowing or guard symbol insertion, the out-of-band emission of GFDM can be efficiently reduced, as compared with orthogonal frequency division multiplexing (OFDM) [1], [3], [4]. It is also more spectral efficient than OFDM in the sense that via the tail biting operation, only one cyclic prefix (CP) is used for each GFDM block that consists of a number of subcarriers and subsymbols, making it particularly attractive for short burst transmission. Therefore, in recent years, GFDM has received much attention, including low complexity implementations [3], [5], [6], filter coefficient optimization designs [7], [8], and combinations with Alamouti and multiple-input multiple-output (MIMO) schemes [9], [10]. To satisfy the requirements of next generation wireless networks, such as commercially affordable and efficient wideband radio design for terminals supporting various high data-rate scenarios, direct-conversion transceivers have become a popular solution due to their desirable characteristics, such as low cost, low power and small size [11], [12]. However, one of the main problems encountered by a direct-conversion structure is the inherent inphase/quadrature (I/Q) imbalance. The imperfections of analog front-end local oscillators (LO) in radio frequency circuits cause the amplitudes of I/Q oscillators to be different and/or the phase shift to deviate from the desired 90°. This results in the so-called self-image interference which reduces the modulation/demodulation accuracy of the transmission systems and degrades the overall system performance considerably.

Various efforts have been made to reduce the I/Q distortions in communication systems which can be classified into data-assisted approaches [13]–[19] and blind ones [20]–[26]. Blind adaptive approaches are particularly attractive due to their trade-off between implementation complexities and I/Q compensation capabilities. These methods typically utilize the so-called 'properness' or 'second order circularity' characteristic inherent to most modern constellation mappings in the sense that I/Q distortions make the desired proper communication signals improper (second order noncircular), which manifests itself in a power mismatch (magnitude imbalance) and/or correlation (phase imbalance) between the I and Q channels [27]–[31]. Therefore, the self-image interference introduced by I/Q

Manuscript received January 4, 2018; revised May 31, 2018; accepted July 18, 2018. Date of publication July 31, 2018; date of current version August 9, 2018. The associate editor coordinating the review of this manuscript and approving it for publication was Dr. Romain Couillet. This work was supported by the National Natural Science Foundation of China under Grants 61720106003 and 61771124. *(Corresponding authors: Yili Xia and Yongming Huang.)*

H. Cheng, Y. Xia, Y. Huang, and L. Yang are with the School of Information Science and Engineering, Southeast University, Nanjing 210096, China (e-mail: haocheng@seu.edu.cn; yili_xia@seu.edu.cn; huangym@seu.edu.cn; lxyang@seu.edu.cn).

D. P. Mandic is with the Department of Electrical and Electronic Engineering, Imperial College London, London SW7 2AZ, U.K. (e-mail: d.mandic@imperial.ac.uk).

Color versions of one or more of the figures in this paper are available online at http://ieeexplore.ieee.org.

Digital Object Identifier 10.1109/TSP.2018.2860556

1053-587X © 2018 IEEE. Personal use is permitted, but republication/redistribution requires IEEE permission.
See http://www.ieee.org/publications_standards/publications/rights/index.html for more information.

imbalance can be mitigated by making the distorted signals proper again. Based on this principle, a complex least mean square (CLMS) adaptive I/Q compensation method was proposed in [21], in which a pre-whitening scheme was implemented to speed up its convergence. This idea has been extended to calibrate frequency-dependent I/Q distortions in both transmitters and receivers for OFDM systems [23], [25]. To perform an intrinsic signal decorrelation within the stochastic weight update process, a normalized complex LMS (NCLMS) adaptive I/Q imbalance compensator for OFDM direct-conversion receivers has been developed in [22], and its theoretical self-image attenuation performance has been justified via the standard variance analysis on its weight error coefficients. Although many solutions have been reported for I/Q imbalance compensation for OFDM systems, this task has just emerged in GFDM systems [32], [33], and both a theoretical evaluation on its impacts on GFDM receivers and a blind compensation solution are still lacking in the literature.

To this end, we first quantify the performance deterioration, resulting from I/Q distortions, on GFDM receivers, via a rigorous signal-to-interference plus noise ratio (SINR) analysis. An NCLMS based blind adaptive I/Q imbalance compensator is next proposed. In order to provide detailed intrinsic physics on its compensation capability, we argue that the currently adopted mean square (variance) analysis provides limited physical insights into the statistical behavior of the compensator, since the improperness of its weight error also arises due to that of the I/Q imbalanced received signal, an issue that has been systematically omitted so far. Therefore, following on recent advances in augmented complex statistics [34]–[36], a full second order performance analysis is conducted to quantify the evolutions of both the standard variance and complementary variance of the weight error coefficient in the transient and steady state stages. This makes it possible to also quantify the individual I/Q imbalance compensation contributions theoretically, in terms of image rejection ratio (IRR) from its I and Q channels. This aspect is still missing in the literature and is not possible to address by using the conventional variance analysis only. This analysis also facilitates rigorous evaluations of SINR improvements by NCLMS for GFDM receivers. Simulation results on GFDM waveforms support the analysis.

Notation: Scalar quantities, column vectors and matrices are denoted by normal letters, a, boldface lowercase letters, $\mathbf{a}$, and boldface uppercase letters, $\mathbf{A}$, respectively. An $N \times N$ identity matrix is denoted by $\mathbf{I}_N$. The superscripts $(\cdot)^T$, $(\cdot)^*$ and $(\cdot)^H$ are respectively the transpose, complex conjugate and Hermitian transpose operators. The symbol $E[\cdot]$ denotes the statistical expectation. The subscripts $(\cdot)_r$ and $(\cdot)_j$ respectively extract the real part and the imaginary part of its argument, and $j = \sqrt{-1}$. The symbol $[\mathbf{A}]_{l,p}$ denotes the element at the lth row and the pth column of matrix $\mathbf{A}$.

II. System Model

We consider a typical GFDM system with K subcarriers which transmit a zero-mean data vector of N 2^L-QAM modulated subsymbols $\mathbf{s} = [s(0), s(1), \ldots, s(N-1)]^T$, with a covariance matrix $E[\mathbf{s}\mathbf{s}^H] = \sigma_s^2 \mathbf{I}_N$, over a wireless multipath channel. Within the GFDM transmitter, the data vector $\mathbf{s}$ is divided into K subvectors, so that, $\mathbf{s} = [\mathbf{s}_0^T, \mathbf{s}_1^T, \ldots, \mathbf{s}_{K-1}^T]^T$. Each subvector $\mathbf{s}_k$ contains M elements, that is, $\mathbf{s}_k = [s_{kM}, s_{kM+1}, \ldots, s_{kM+M-1}]^T$, where $k = 0, 1, \ldots, K-1$ and $N = MK$. In this way, data $s_{kM+m}, m = 0, \ldots, M-1$ refers to the mth subsymbol to be transmitted on the kth subcarrier within the GFDM transmitter. It is then upsampled by the factor of K, circularly convoluted with the pulse shaping filter $g(n)$ at time instant n, and up-converted to the corresponding subcarrier frequency. The output samples of all K subcarriers and M time slots are added together to give a GFDM transmitting signal $x(n)$ in the form [3], [8], [37]

$$x(n) = \sum_{k=0}^{K-1} \sum_{m=0}^{M-1} s_{kM+m} g\big((n - mK)_N\big) e^{j\frac{2\pi kn}{K}}, \quad 0 \le n \le N-1, \tag{1}$$

where $(\cdot)_N$ is the modulo N operation. For compactness, this transmission process can be described in a vector form as [38],

$$\mathbf{x} = \mathbf{A}\mathbf{s}, \tag{2}$$

where $\mathbf{x} = [x(0), x(1), \ldots, x(N-1)]^T$ is the transmitting data vector, and the detailed expression for matrix $\mathbf{A}$ is given by

$$\mathbf{A} = \big[\underbrace{\mathbf{a}_{0,0}, \mathbf{a}_{1,0}, \ldots, \mathbf{a}_{K-1,0}}_{\text{Time slot 1}} \,|\, \underbrace{\mathbf{a}_{0,1}, \mathbf{a}_{1,1}, \ldots, \mathbf{a}_{K-1,1}}_{\text{Time slot 2}} \,| \cdots | \underbrace{\mathbf{a}_{0,M-1}, \mathbf{a}_{1,M-1}, \ldots, \mathbf{a}_{K-1,M-1}}_{\text{Time slot } M}\big], \tag{3}$$

where $\mathbf{a}_{k,m} = [a_{k,m}(0), a_{k,m}(1), \ldots, a_{k,m}(N-1)]^T$ and $a_{k,m}(n) = g((n - mK)_N) e^{j\frac{2\pi kn}{K}}$. In addition, when $M = 1$, matrix $\mathbf{A}$ simplifies into an N-point unitary Discrete Fourier Transform (DFT) matrix $\mathbf{W}_N$, where $[\mathbf{W}_N]_{k,l} = e^{-j\frac{2\pi kl}{N}}, k, l = 0, 1, \ldots, N-1$, and the GFDM system reduces into an OFDM system with $\mathbf{x} = \mathbf{W}_N \mathbf{s}$ [8]. The cyclic prefix (CP) is added to $\mathbf{x}$ before transmission to eliminate the inter-symbol interference (ISI) caused by multipath propagation. On the receiver side, after down-conversion and CP removal, the ideal digital data vector $\mathbf{r}$ in the baseband is given by

$$\mathbf{r} = \mathbf{H}\mathbf{x} + \mathbf{q} = \mathbf{H}\mathbf{A}\mathbf{s} + \mathbf{q}, \tag{4}$$

where $\mathbf{r} = [r(0), r(1), \ldots, r(N-1)]^T$, $\mathbf{H}$ represents the circulant channel matrix and $\mathbf{q}$ is the zero-mean additive white Gaussian noise with a covariance matrix $E[\mathbf{q}\mathbf{q}^H] = \sigma_q^2 \mathbf{I}_N$. The wireless channel is considered to be static frequency-selective, so that it can be modeled as a linear time invariant system and the wide sense stationarity of the received data $\mathbf{r}$ is guaranteed. However, the imperfections of the local oscillator within the receiver introduce I/Q mismatches, which results in a self-image interference within $\mathbf{r}$, so that the received data vector under I/Q imbalance is in a widely linear form [16], [21], [22]

$$\mathbf{y} = \alpha \mathbf{r} + \beta \mathbf{r}^*, \tag{5}$$

where

$$\alpha = \frac{1 + (1+\varepsilon)e^{-j\theta}}{2}, \tag{6}$$

$$\beta = \frac{1 - (1+\varepsilon)e^{j\theta}}{2}, \tag{7}$$

and ε and θ respectively denote the amplitude and phase mismatches; due to the underlying physics of the down-conversion operation, we have $\alpha + \beta^* = 1$. Therefore, for the purpose of blind I/Q imbalance compensation, it is equivalent to consider

$$\mathbf{y} = \mathbf{z} + \lambda \mathbf{z}^*, \tag{8}$$

where $\mathbf{z} = \alpha \mathbf{r}$ is the I/Q imbalance-free received data vector and $\lambda = \frac{\beta}{\alpha^*}$ is the imbalance coefficient.

III. SINR Analysis on I/Q Imbalanced GFDM Receivers

We next investigate the impacts of I/Q imbalance on the transmission quality of GFDM receivers via a rigorous SINR analysis. Firstly, by substituting (4) into (5), the received data vector $\mathbf{y}$ is expanded as

$$\mathbf{y} = \alpha \mathbf{H}\mathbf{A}\mathbf{s} + \beta \mathbf{H}^* \mathbf{A}^* \mathbf{s}^* + \alpha \mathbf{q} + \beta \mathbf{q}^*. \tag{9}$$

By considering a zero forcing (ZF) equalization with a perfect channel estimation in time domain, a detected data vector $\hat{\mathbf{y}}$ can be expressed as

$$\hat{\mathbf{y}} = \mathbf{H}^{-1}\mathbf{y} = \alpha \mathbf{A}\mathbf{s} + \beta \mathbf{H}^{-1}\mathbf{H}^*\mathbf{A}^*\mathbf{s}^* + \alpha \mathbf{H}^{-1}\mathbf{q} + \beta \mathbf{H}^{-1}\mathbf{q}^*. \tag{10}$$

After equalization, by using a receiver filter matrix $\mathbf{G} \in \mathbb{C}^{N\times N}$, the estimated symbol data $\hat{\mathbf{s}}$ under I/Q imbalance can be obtained as

$$\begin{aligned}\hat{\mathbf{s}} &= \mathbf{G}\hat{\mathbf{y}} \\ &= \alpha \mathbf{G}\mathbf{A}\mathbf{s} + \beta \mathbf{G}\mathbf{H}^{-1}\mathbf{H}^*\mathbf{A}^*\mathbf{s}^* + \alpha \mathbf{G}\mathbf{H}^{-1}\mathbf{q} + \beta \mathbf{G}\mathbf{H}^{-1}\mathbf{q}^*.\end{aligned} \tag{11}$$

We consider two typical GFDM receivers, matched filter (MF) receivers and zero forcing (ZF) ones, which either aim at maximizing the signal to noise ratio (SNR) or at eliminating the interference caused by the non-orthogonality of GFDM [39].

A. Matched Filter (MF) Receiver

For an MF receiver, we have $\mathbf{G} = \mathbf{A}^H$ and the estimated signal $\hat{\mathbf{s}}$ in (11) now becomes

$$\begin{aligned}\hat{\mathbf{s}} = {}& \alpha \mathbf{A}^H\mathbf{A}\mathbf{s} + \beta \mathbf{A}^H\mathbf{H}^{-1}\mathbf{H}^*\mathbf{A}^*\mathbf{s}^* \\ &+ \alpha \mathbf{A}^H\mathbf{H}^{-1}\mathbf{q} + \beta \mathbf{A}^H\mathbf{H}^{-1}\mathbf{q}^*,\end{aligned} \tag{12}$$

After defining

$$\mathbf{B} = \mathbf{H}^{-1}\mathbf{H}^*\mathbf{A}^*, \tag{13}$$

and

$$\mathbf{q}_1 = \alpha \mathbf{A}^H\mathbf{H}^{-1}\mathbf{q} + \beta \mathbf{A}^H\mathbf{H}^{-1}\mathbf{q}^*, \tag{14}$$

from (12), we obtain the nth estimated subsymbol $\hat{s}(n)$ as

$$\begin{aligned}\hat{s}(n) = {}& \alpha[\mathbf{A}^H\mathbf{A}]_{n,n}s(n) + \alpha \sum_{p=0,p\neq n}^{N-1}[\mathbf{A}^H\mathbf{A}]_{n,p}s(p) \\ &+ \beta \sum_{p=0}^{N-1}[\mathbf{A}^H\mathbf{B}]_{n,p}s^*(p) + q_1(n),\end{aligned} \tag{15}$$

where $q_1(n)$ is the nth element of $\mathbf{q}_1$. Now, using the GFDM modulation matrix $\mathbf{A}$ in (3) and defining $\mathbf{b}_p$ as the pth column vector within matrix $\mathbf{B}$, the estimated subsymbol $\hat{s}(n)$ in (15) simplifies into

$$\begin{aligned}\hat{s}(n) = {}& \underbrace{\alpha \mathbf{a}_n^H\mathbf{a}_n s(n)}_{S(n)} + \underbrace{\alpha \sum_{p=0,p\neq n}^{N-1}\mathbf{a}_n^H\mathbf{a}_p s(p)}_{I(n)} \\ &+ \underbrace{\beta \sum_{p=0}^{N-1}\mathbf{a}_n^H\mathbf{b}_p s^*(p)}_{P(n)} + q_1(n),\end{aligned} \tag{16}$$

where $\mathbf{a}_n$ refers to $\mathbf{a}_{k,m}$, since $n = mM + k$. Note that on the right hand side (RHS) of (16), the component $S(n)$ contains the desired signal $s(n)$, $I(n)$ represents the interference leaked from other subsymbols due to the non-orthogonal property of GFDM, and $P(n)$ includes all the self images introduced by the receiver I/Q imbalance. The average noise power aggregated over a GFDM block can be evaluated as

$$\begin{aligned}&\sum_{n=0}^{N-1}E[|q_1(n)|^2] \\ &\quad = |\alpha|^2 \mathrm{tr}\{E[\mathbf{A}^H\mathbf{H}^{-1}\mathbf{q}(\mathbf{A}^H\mathbf{H}^{-1}\mathbf{q})^H]\} \\ &\qquad + |\beta|^2 \mathrm{tr}\{E[\mathbf{A}^H\mathbf{H}^{-1}\mathbf{q}^*(\mathbf{A}^H\mathbf{H}^{-1}\mathbf{q}^*)^H]\} \\ &\quad = (|\alpha|^2 + |\beta|^2)\sigma_q^2 \mathrm{tr}\{\mathbf{A}^H\mathbf{H}^{-1}(\mathbf{A}^H\mathbf{H}^{-1})^H\} \\ &\quad = (|\alpha|^2 + |\beta|^2)\sigma_q^2 \sum_{n=0}^{N-1}\sum_{p=0}^{N-1}\left|[\mathbf{A}^H\mathbf{H}^{-1}]_{n,p}\right|^2,\end{aligned} \tag{17}$$

where $\mathrm{tr}\{\cdot\}$ is the matrix trace operator. The SINR, defined as the power ratio between the desired signal and all the interference plus noise [37], [40], of an MF receiver over a whole GFDM data block, is then given by

$$\mathrm{SINR}^{\mathrm{MF}} \triangleq \frac{\sum_{n=0}^{N-1}E[|S(n)|^2]}{\sum_{n=0}^{N-1}E[|I(n)|^2] + \sum_{n=0}^{N-1}E[|P(n)|^2] + \sum_{n=0}^{N-1}E[|q_1(n)|^2]}.$$

From (16) and (17) and after a few mathematical manipulations, $\mathrm{SINR}^{\mathrm{MF}}$ can be mathematically reformulated as in (18), shown at the bottom of the next page, where $\mathrm{SNR} \triangleq E[|s(n)|^2]/E[|q(n)|^2] = \sigma_s^2/\sigma_q^2$ is the system SNR.

B. Zero Forcing (ZF) Receiver

For a ZF receiver we have $\mathbf{G} = \mathbf{A}^{-1}$, and from (11), the estimated signal $\hat{\mathbf{s}}$ now becomes

$$\hat{\mathbf{s}} = \alpha\mathbf{s} + \beta\mathbf{A}^{-1}\mathbf{H}^{-1}\mathbf{H}^{*}\mathbf{A}^{*}\mathbf{s}^{*} + \alpha\mathbf{A}^{-1}\mathbf{H}^{-1}\mathbf{q} + \beta\mathbf{A}^{-1}\mathbf{H}^{-1}\mathbf{q}^{*}. \tag{19}$$

A comparison of the first terms on the RHS of (19) and (12) shows that the interference from other subsymbols and subcarriers has been removed due to the characteristics of ZF receivers. Upon further defining

$$\mathbf{q}_2 = \alpha\mathbf{A}^{-1}\mathbf{H}^{-1}\mathbf{q} + \beta\mathbf{A}^{-1}\mathbf{H}^{-1}\mathbf{q}^{*}, \tag{20}$$

the estimate of the nth subsymbol $\hat{s}(n)$ becomes

$$\hat{s}(n) = \underbrace{\alpha s(n)}_{S(n)} + \underbrace{\beta\sum_{p=0}^{N-1}[\mathbf{A}^{-1}\mathbf{B}]_{n,p}s^{*}(p) + q_2(n)}_{P(n)}, \tag{21}$$

where $q_2(n)$ is the nth element of $\mathbf{q}_2$ and its aggregated power is given by

$$\sum_{n=0}^{N-1}E[|q_2(n)|^2] = (|\alpha|^2 + |\beta|^2)\sigma_q^2\sum_{n=0}^{N-1}\sum_{p=0}^{N-1}\left|[\mathbf{A}^{-1}\mathbf{H}^{-1}]_{n,p}\right|^2. \tag{22}$$

Based on (21), the SINR of a ZF receiver over the whole GFDM block can be defined as

$$\text{SINR}^{\text{ZF}} \triangleq \frac{\sum_{n=0}^{N-1}E[|S(n)|^2]}{\sum_{n=0}^{N-1}E[|P(n)|^2] + \sum_{n=0}^{N-1}E[|q_2(n)|^2]},$$

and after some algebraic manipulations, the final expression of SINR^{ZF} can be obtained as

$$\text{SINR}^{\text{ZF}} = \frac{N}{|\lambda|^2\sum_{n=0}^{N-1}\sum_{p=0}^{N-1}|[\mathbf{A}^{-1}\mathbf{B}]_{n,p}|^2 + \frac{1+|\lambda|^2}{\text{SNR}}\sum_{n=0}^{N-1}\sum_{p=0}^{N-1}\left|[\mathbf{A}^{-1}\mathbf{H}^{-1}]_{n,p}\right|^2}. \tag{23}$$

Equations (18) and (23) now establish the closed-form explanations on how I/Q imbalance deteriorates the SINR performance of GFDM receivers via the imbalance coefficient λ. From (14) and (20), also observe that due to the filtering process of GFDM and the multipath channel effect, system noises in both the MF and ZF receivers become colored.

IV. Normalized Complex LMS (NCLMS) Adaptive I/Q Imbalance Compensator

It is important to note that at time instant n, or equivalently, at the nth subsymbol, based on (8), there exists a weight coefficient $w(n)$ which allows us to perform the signal transformation

$$\begin{aligned} &y(n) - w^{*}(n)y^{*}(n) \\ &\quad = (1 - w^{*}(n)\lambda^{*})z(n) + (\lambda - w^{*}(n))z^{*}(n). \end{aligned} \tag{24}$$

Now, the self-image component $z^{*}(n)$, introduced by the I/Q mismatches at the receiver, can be eliminated when the second term on the RHS vanishes, or equivalently, $w(n) \to \lambda^{*}$ as $n \to \infty$. As discussed in [22], by treating $z^{*}(n)$ as an additional noise to the system, this can be achieved by building up an adaptive noise canceller to minimize the instantaneous power $J(n)$ of a noise residual $e(n)$, where

$$e(n) = y(n) - w^{*}(n)z^{*}(n), \tag{25}$$

$$J(n) = e(n)e^{*}(n) = |e(n)|^2, \tag{26}$$

and a global minimum of $J(n)$ is guaranteed at $w(n) = \lambda^{*}$ only [41]. Therefore, a fast weight update rule, e.g., the normalized complex LMS (NCLMS), can be used for this minimization problem, to give

$$w(n+1) = w(n) + \mu\frac{z^{*}(n)e^{*}(n)}{|z(n)|^2}, \tag{27}$$

where μ is the step-size.

However, in general, $z(n)$ is unknown to the receiver side, and a natural alternative is to use an estimate of $z(n)$ in its place in (27). First, observe that at time instant n, from (8) and its complex conjugate, $z(n)$ can be expressed as

$$z(n) = \frac{y(n) - \lambda y^{*}(n)}{1 - |\lambda|^2}. \tag{28}$$

While, with an appropriate step-size, μ, the weight coefficient, $w(n)$, asymptotically converges to λ^{*} as time evolves. Therefore, a sample estimate of $z(n)$, that is, $\hat{z}(n)$, can be performed as

$$\hat{z}(n) = \frac{y(n) - w^{*}(n)y^{*}(n)}{1 - |w(n)|^2}. \tag{29}$$

Now, by taking $\hat{z}(n)$ in place of $z(n)$ in (25) and (27), we arrive at the final weight update for NCLMS adaptive I/Q imbalance compensator, given by [22]

$$w(n+1) = w(n) + \mu\frac{\hat{z}^{*}(n)\hat{e}^{*}(n)}{|\hat{z}(n)|^2}, \tag{30}$$

where

$$\hat{e}(n) = y(n) - w^{*}(n)\hat{z}^{*}(n). \tag{31}$$

$$\text{SINR}^{\text{MF}} = \frac{\sum_{n=0}^{N-1}|\mathbf{a}_n^H\mathbf{a}_n|^2}{\sum_{n=0}^{N-1}\sum_{p=0,p\neq n}^{N-1}|\mathbf{a}_n^H\mathbf{a}_p|^2 + |\lambda|^2\sum_{n=0}^{N-1}\sum_{p=0}^{N-1}|\mathbf{a}_n^H\mathbf{b}_p|^2 + \frac{1+|\lambda|^2}{\text{SNR}}\sum_{n=0}^{N-1}\sum_{p=0}^{N-1}\left|[\mathbf{A}^H\mathbf{H}^{-1}]_{n,p}\right|^2} \tag{18}$$

V. Full Second Order Performance Analysis of the Proposed NCLMS Compensator

For most practical complex-valued constellation mappings, e.g., 2^L-QAM, the received signal without I/Q imbalance, that is, $z(n)$, is second order circular (proper), characterized by a vanishing complementary variance $\widetilde{\sigma}_z^2 = E[z^2(n)] = 0$, and the full second order statistics of $z(n)$ are completely described by its variance, $\sigma_z^2 = E[|z(n)|^2]$ [21]–[26]. On the other hand, as shown in (8), the received signal under I/Q imbalance, that is, $y(n)$, admits a widely linear form on both $z(n)$ and its self-image $z^*(n)$, and its complementary variance $\widetilde{\sigma}_y^2$ can be evaluated from (8) as $\widetilde{\sigma}_y^2 = E[y^2(n)] = 2\lambda\sigma_z^2$, which indicates a certain degree of improperness [27]–[31]. Therefore, from the second order statistical perspective, the idea behind the considered NCLMS compensator is to iteratively calibrate the original improper signal to be proper again, i.e., for the improperness of $\hat{z}(n)$ to vanish after the compensation process.

A. Full Second Order Convergence Analysis

It is natural to investigate whether the so-introduced signal improperness propagates into the compensator via (30) and (31) during its convergence. To address this issue, we first define the weight error coefficient $\varphi(n)$ as

$$\varphi(n) = w(n) - \lambda^*, \tag{32}$$

and introduce the complementary variance $\widetilde{\kappa}(n) = E[\varphi^2(n)]$ to justify its improperness [34]–[36]. From (30) and (31), the update of weight error $\varphi(n)$ is given by

$$\varphi(n+1) = (1-\mu)\varphi(n) + \mu\frac{\hat{z}^*(n)e_{\mathrm{o}}^*(n)}{|\hat{z}(n)|^2}, \tag{33}$$

where

$$e_{\mathrm{o}}(n) = y(n) - \lambda\hat{z}^*(n). \tag{34}$$

Upon squaring both sides of (33) and taking the statistical expectation $E[\cdot]$, the evolution of the weight error complementary variance, $\widetilde{\kappa}(n)$, is obtained as

$$\begin{aligned}\widetilde{\kappa}(n+1) = (1-\mu)^2\widetilde{\kappa}(n) + \mu^2 E\left[\left(\frac{\hat{z}^*(n)e_{\mathrm{o}}^*(n)}{|\hat{z}(n)|^2}\right)^2\right] \\ + 2\mu(1-\mu)E\left[\varphi(n)\frac{\hat{z}^*(n)e_{\mathrm{o}}^*(n)}{|\hat{z}(n)|^2}\right],\end{aligned} \tag{35}$$

where, upon employing the standard assumption commonly used in blind equalization analysis that the weight error $\varphi(n)$ is statistically independent of $y(n)$ [42], [43], and a further independence assumption between $\varphi(n)$ and $\hat{z}(n)$, typically used to ease the mathematical tractability of adaptive I/Q imbalance compensator [22], [44], the third term on the RHS can be approximately evaluated as

$$E\left[\varphi(n)\frac{\hat{z}^*(n)e_{\mathrm{o}}^*(n)}{|\hat{z}(n)|^2}\right] \approx E\left[\varphi(n)\right]E\left[\frac{\hat{z}^*(n)e_{\mathrm{o}}^*(n)}{|\hat{z}(n)|^2}\right]. \tag{36}$$

Due to the asymptotically unbiased nature of NCLMS [22], this term vanishes, together with $E[\varphi(n)]$, as time evolves. This unbiased nature also implies that $e_{\mathrm{o}}(n)$ approaches $\hat{z}(n)$ and $\hat{z}(n)$ approaches $z(n)$ when $n \to \infty$, thus facilitating an approximate evaluation of the second term on the RHS of (35) in the form

$$\begin{aligned}E\left[\left(\frac{\hat{z}^*(n)e_{\mathrm{o}}^*(n)}{|\hat{z}(n)|^2}\right)^2\right] &\approx E\left[\left(\frac{\hat{z}^*(n)}{|\hat{z}(n)|}\right)^4\right] \approx E\left[\left(\frac{z^*(n)}{|z(n)|}\right)^4\right] \\ &\approx 0,\end{aligned} \tag{37}$$

The last step above stems from the strict circularity[1] of $z(n)/|z(n)|$. Therefore, the evolution of $\widetilde{\kappa}(n)$ in (35) now simplifies into

$$\widetilde{\kappa}(n+1) = (1-\mu)^2\widetilde{\kappa}(n). \tag{38}$$

Correspondingly, the evolution of the standard weight error variance $\kappa(n)$, defined as $\kappa(n) = E[|\varphi(n)|^2]$, can be obtained as [22]

$$\kappa(n+1) = (1-\mu)^2\kappa(n) + \mu^2. \tag{39}$$

Remark 1: Equations (38) and (39) together provide the full second order statistical evolution of the weight error $\varphi(n)$, from which it can be verified that the unified bound on the step-size μ to guarantee the convergence[2] of both $\widetilde{\kappa}(n)$ and $\kappa(n)$ is $0 < \mu < 2$.

B. Full Second Order Steady State Analysis

Suppose that μ is chosen such that the convergence of $\widetilde{\kappa}(n)$ and $\kappa(n)$ is guaranteed. Then, at the steady state, i.e., $n \to \infty$, from (38) and (39), we have

$$\widetilde{\kappa}(\infty) = 0,\ \kappa(\infty) = \frac{\mu}{2-\mu}, \tag{40}$$

Remark 2: The improperness of the weight error $\varphi(n)$ vanishes at the steady state, as evidenced by $\widetilde{\kappa}(\infty) = 0$, independent of how its initialization, $\varphi(0)$, is performed. Physically, as a byproduct of the iterative calibration on the improperness of the compensated signal $\hat{z}(n)$, the improperness of $\varphi(n)$ has also been compensated for. On the other hand, for $0 < \mu < 2$, the weight error variance $\kappa(\infty)$ is a monotonically increasing function of the step-size μ.

An important application of the proposed full second order statistical analysis lies in the fact that it also provides enough degrees of freedom to quantify the second order performance of the real (I) and imaginary (Q) channels within the proposed NCLMS compensator, individually. This becomes clear when $\varphi(n)$ is rewritten in terms of its real and imaginary components

[1] When the underlying transmission scheme has a multi-carrier nature, the second order circular variable $z(n)$ is Gaussian distributed [45]. Therefore, by defining a random variable $z(n)/|z(n)| = e^{j\phi(n)}$, its phase $\phi(n)$ is uniformly distributed over [0, 2π) [46], indicating the strictly circular nature of $e^{j\phi(n)}$ (equivalently, $z(n)/|z(n)|$). For a strictly circular random variable $z(n)/|z(n)|$, we further have $E[(z(n)/|z(n)|)^4] = 0$ [28], and hence, $E[(z^*(n)/|z(n)|)^4] = 0$.

[2] Strictly speaking, we are not able to talk about the convergence of a complex-valued variable, like $\widetilde{\kappa}(n)$, since the complex domain is not ordered. However, the real-valued nature of the transition coefficient $(1-\mu)^2$ in (38) guarantees that the real and imaginary parts of $\widetilde{\kappa}(n)$, that is, $\widetilde{\kappa}_r(n)$ and $\widetilde{\kappa}_j(n)$, converge independently.

as $\varphi(n) = \varphi_r(n) + j\varphi_j(n)$. Accordingly, its standard and complementary variances become

$$\kappa(n) = E\left[\varphi_r^2(n)\right] + E\left[\varphi_j^2(n)\right], \tag{41}$$

$$\widetilde{\kappa}(n) = E\left[\varphi_r^2(n)\right] - E\left[\varphi_j^2(n)\right] + 2jE\left[\varphi_r(n)\varphi_j(n)\right]. \tag{42}$$

Upon the inspection of both sides of (41) and (42), we have

$$E\left[\varphi_r^2(n)\right] = \frac{\kappa(n) + \widetilde{\kappa}_r(n)}{2}, E\left[\varphi_j^2(n)\right] = \frac{\kappa(n) - \widetilde{\kappa}_r(n)}{2}, \tag{43}$$

and

$$E\left[\varphi_r(n)\varphi_j(n)\right] = \frac{\widetilde{\kappa}_j(n)}{2j}. \tag{44}$$

Now, a joint consideration of (38), (39), (43) and (44), enables decoupling the convergence of the weight error variances in both the I and Q channels within the compensator, that is, $E[\varphi_r^2(n)]$ and $E[\varphi_j^2(n)]$, as well as their cross term $E[\varphi_r(n)\varphi_j(n)]$. Importantly, this property cannot be achieved by using the conventional real-valued variance analysis in [22], on the weight error coefficient $\varphi(n)$ only, due to its single degree of freedom.

In the steady state, i.e., $n \to \infty$, by substituting (40) into (43) and (44), we obtain

$$E\left[\varphi_r^2(\infty)\right] = E\left[\varphi_j^2(\infty)\right] = \frac{\kappa(\infty)}{2}, \tag{45}$$

and

$$E\left[\varphi_r(\infty)\varphi_j(\infty)\right] = 0. \tag{46}$$

Remark 3: Equations (45) and (46) illustrate that the NCLMS compensator equally assigns the total weight error variance $E[\varphi^2(\infty)]$ to its I and Q channels at the steady state stage. Also both channels are uncorrelated, as a result of the properness of $\varphi(\infty)$.

C. Steady State IRR Analysis

The conventional metric for the evaluation of an I/Q imbalance compensation scheme is the so-called image rejection ratio (IRR), defined as the power ratio between the desired signal and its self-image interference [47]. According to (24), the IRR of NCLMS at time instant n, denoted by IRR(n), is given by

$$\begin{aligned}\mathrm{IRR}(n) &\triangleq \frac{E[|(1 - w^*(n)\lambda^*)z(n)|^2]}{E[|(\lambda - w^*(n))z^*(n)|^2]} \\ &= \frac{E[|1 - w^*(n)\lambda^*|^2]}{E[|\lambda - w^*(n)|^2]},\end{aligned} \tag{47}$$

where the last step is performed by considering the statistical independence between $w(n)$ and $z(n)$. Observe that, in the steady state, according to (32), the denominator of IRR(∞) is in fact $\kappa(\infty)$ from (40). Next, based on the asymptotically unbiased nature of NCLMS, that is, $E[\varphi(\infty)] = 0$, the numerator of IRR(∞) can be further evaluated as

$$\begin{aligned}&E[|1 - w^*(\infty)\lambda^*|^2] \\ &\quad = (1 - |\lambda|^2)^2 + |\lambda|^2 E[|\varphi(\infty)|^2] \\ &\qquad - (1 - |\lambda|^2)E[\varphi^*(\infty)\lambda^* + \varphi(\infty)\lambda] \\ &\quad = (1 - |\lambda|^2)^2 + |\lambda|^2\kappa(\infty),\end{aligned} \tag{48}$$

and hence,

$$\mathrm{IRR}(\infty) = \frac{(1 - |\lambda|^2)^2}{\kappa(\infty)} + |\lambda|^2. \tag{49}$$

Remark 4: A joint consideration of equations (45) and (49) illustrates that although the overall self-image cancellation capability of the NCLMS compensator is dependent on the exact amount of I/Q imbalance within the receiver, its I and Q channels always yield identical contributions.

It is then natural to ask whether there exists a measurement to provide more interpretable intrinsic physics of the I and Q channels within an I/Q imbalanced receiver and the proposed compensator. To address this issue, we first rewrite λ, $w(n)$ and $z(n)$ on the RHS of (24) in terms of their real and imaginary parts, and after a few manipulations, we have

$$\begin{aligned}&y(n) - w^*(n)y^*(n) \\ &\quad = (1 + w_j(n)\lambda_j - w_r(n)\lambda_r + \lambda_r - w_r(n))z_r(n) \\ &\qquad + (\lambda_j + w_j(n) - w_r(n)\lambda_j - w_j(n)\lambda_r)z_j(n) \\ &\qquad + j(1 + w_j(n)\lambda_j - w_r(n)\lambda_r - \lambda_r + w_r(n))z_j(n) \\ &\qquad + j(\lambda_j + w_j(n) + w_r(n)\lambda_j + w_j(n)\lambda_r)z_r(n).\end{aligned} \tag{50}$$

Now, based on the physical meaning of image rejection ratio (IRR) in (47), from (50), we are able to define individual IRRs along I and Q channels of NCLMS respectively as

$$\begin{aligned}&\mathrm{IRR}_I(n) \\ &\triangleq \frac{E[((1 + w_j(n)\lambda_j - w_r(n)\lambda_r + \lambda_r - w_r(n))z_r(n))^2]}{E[((\lambda_j + w_j(n) - w_r(n)\lambda_j - w_j(n)\lambda_r)z_j(n))^2]},\end{aligned} \tag{51}$$

$$\begin{aligned}&\mathrm{IRR}_Q(n) \\ &\triangleq \frac{E[((1 + w_j(n)\lambda_j - w_r(n)\lambda_r + w_r(n) - \lambda_r)z_j(n))^2]}{E[((\lambda_j + w_j(n) + w_r(n)\lambda_j + w_j(n)\lambda_r)z_r(n))^2]}.\end{aligned} \tag{52}$$

Considering both the statistical independence between $w(n)$ and $z(n)$ and the properness of $z(n)$, e.g., $E[z_r^2(n)] = E[z_j^2(n)]$, we can simplify (51) and (52) as

$$\mathrm{IRR}_I(n) = \frac{E[(1 + w_j(n)\lambda_j - w_r(n)\lambda_r + \lambda_r - w_r(n))^2]}{E[(\lambda_j + w_j(n) - w_r(n)\lambda_j - w_j(n)\lambda_r)^2]}, \tag{53}$$

$$\mathrm{IRR}_Q(n) = \frac{E[(1 + w_j(n)\lambda_j - w_r(n)\lambda_r + w_r(n) - \lambda_r)^2]}{E[(\lambda_j + w_j(n) + w_r(n)\lambda_j + w_j(n)\lambda_r)^2]}. \tag{54}$$

Therefore, before performing the considered blind I/Q imbalance compensation procedure, i.e., $w_r(0) = w_j(0) = 0$, the

IRRs of the I and Q channels within an I/Q imbalanced GFDM receiver are respectively given by

$$\mathrm{IRR}_I(0) = \frac{(1+\lambda_r)^2}{\lambda_j^2},\ \ \mathrm{IRR}_Q(0) = \frac{(1-\lambda_r)^2}{\lambda_j^2}. \tag{55}$$

In order to investigate the situations in both channels after the proposed I/Q imbalance compensation, that is for $n \to \infty$, from (32), we have

$$w_r(\infty) = \varphi_r(\infty) + \lambda_r,\ \ w_j(\infty) = \varphi_j(\infty) - \lambda_j. \tag{56}$$

A substitution of (56) into (53) and (54) yields

$$\mathrm{IRR}_I(\infty) = \frac{E[(1-|\lambda|^2-(1+\lambda_r)\varphi_r(\infty)+\lambda_j\varphi_j(\infty))^2]}{E[((1-\lambda_r)\varphi_j(\infty)-\lambda_j\varphi_r(\infty))^2]}, \tag{57}$$

$$\mathrm{IRR}_Q(\infty) = \frac{E[(1-|\lambda|^2+(1-\lambda_r)\varphi_r(\infty)+\lambda_j\varphi_j(\infty))^2]}{E[((1+\lambda_r)\varphi_j(\infty)+\lambda_j\varphi_r(\infty))^2]}. \tag{58}$$

Observe that the term in the numerator of $\mathrm{IRR}_I(\infty)$ in (57) can be further evaluated as

$$\begin{aligned} &E[(1-|\lambda|^2-(1+\lambda_r)\varphi_r(\infty)+\lambda_j\varphi_j(\infty))^2] \\ &\quad = (1-|\lambda|^2)^2 + (1+\lambda_r)^2 E[\varphi_r^2(\infty)] + \lambda_j^2 E[\varphi_j^2(\infty)] \\ &\qquad - 2(1-|\lambda|^2)(1+\lambda_r)E[\varphi_r(\infty)] \\ &\qquad + 2\lambda_j(1-|\lambda|^2)E[\varphi_j(\infty)] \\ &\qquad - 2\lambda_j(1+\lambda_r)E[\varphi_r(\infty)\varphi_j(\infty)] \\ &\quad = (1-|\lambda|^2)^2 + \frac{(1+2\lambda_r+|\lambda|^2)\kappa(\infty)}{2}, \end{aligned} \tag{59}$$

where the last step stems from the asymptotically unbiased nature of NCLMS, i.e., $E[\varphi_r(\infty)] = E[\varphi_j(\infty)] = 0$, and the full second order analysis results in (45) and (46).

In a similar way, after a few mathematical manipulations, we have

$$\begin{aligned} &E[((1-\lambda_r)\varphi_j(\infty)-\lambda_j\varphi_r(\infty))^2] \\ &\quad = \frac{(1-2\lambda_r+|\lambda|^2)\kappa(\infty)}{2}, \end{aligned} \tag{60}$$

$$\begin{aligned} &E[(1-|\lambda|^2+(1-\lambda_r)\varphi_r(\infty)+\lambda_j\varphi_j(\infty))^2] \\ &\quad = (1-|\lambda|^2)^2 + \frac{(1-2\lambda_r+|\lambda|^2)\kappa(\infty)}{2}, \end{aligned} \tag{61}$$

$$\begin{aligned} &E[((1+\lambda_r)\varphi_j(\infty)+\lambda_j\varphi_r(\infty))^2] \\ &\quad = \frac{(1+2\lambda_r+|\lambda|^2)\kappa(\infty)}{2}. \end{aligned} \tag{62}$$

Upon substituting (59), (60), (61), and (62) back into (57) and (58), the closed-form expressions of $\mathrm{IRR}_I(\infty)$ and $\mathrm{IRR}_Q(\infty)$ are obtained as

$$\mathrm{IRR}_I(\infty) = \frac{2(1-|\lambda|^2)^2 + (1+2\lambda_r+|\lambda|^2)\kappa(\infty)}{(1-2\lambda_r+|\lambda|^2)\kappa(\infty)}, \tag{63}$$

$$\mathrm{IRR}_Q(\infty) = \frac{2(1-|\lambda|^2)^2 + (1-2\lambda_r+|\lambda|^2)\kappa(\infty)}{(1+2\lambda_r+|\lambda|^2)\kappa(\infty)}. \tag{64}$$

Remark 5: Both $\mathrm{IRR}_I(\infty)$ and $\mathrm{IRR}_Q(\infty)$ are monotonically decreasing functions of $\kappa(\infty)$, and consequently, also the step-size μ. This indicates that a smaller μ of NCLMS enables better self-image attenuation along both the I and Q channels. In general, the I/Q imbalance introduces unequal amounts of self-interference components into I and Q channels, by comparing $\mathrm{IRR}_I(0)$ and $\mathrm{IRR}_Q(0)$ in (55). This situation still exists after performing the proposed compensation, as evidenced by the different expressions for $\mathrm{IRR}_I(\infty)$ and $\mathrm{IRR}_Q(\infty)$, although both channels contribute equally to the overall self-image cancellation performance of NCLMS, as discussed in *Remark 4*. However, a special class of I/Q mismatches with $\lambda_r = 0$ removes these inequalities, making $\mathrm{IRR}_I(0) = \mathrm{IRR}_Q(0)$ and $\mathrm{IRR}_I(\infty) = \mathrm{IRR}_Q(\infty)$. Based on the analysis in Appendix A, this occurs when the GFDM receiver suffers a certain amount of phase mismatch, θ, only between its I and Q channels, without any amplitude mismatch, i.e., $\varepsilon = 0$.

D. SINR Analysis of I/Q Imbalance Compensated GFDM Receivers

We next evaluate the SINR performance of I/Q imbalance compensated GFDM receivers, with the recovered data obtained by performing the signal transformation in (24) on $\mathbf{y}$ in (9) and its complex conjugate $\mathbf{y}^*$ with $w^*(\infty)$ of NCLMS. After the ZF equalization, the estimated data vector $\hat{\mathbf{s}}$ of a matched filter (MF) receiver can be obtained as

$$\begin{aligned} \hat{\mathbf{s}} &= \mathbf{A}^H\mathbf{H}^{-1}(\mathbf{y} - w^*(\infty)\mathbf{y}^*) \\ &= (1-w^*(\infty)\lambda^*)\alpha\mathbf{A}^H\mathbf{A}\mathbf{s} + (\lambda - w^*(\infty))\alpha^*\mathbf{A}^H\mathbf{H}^{-1}\mathbf{H}^*\mathbf{A}^*\mathbf{s}^* \\ &\quad + (1-w^*(\infty)\lambda^*)\alpha\mathbf{A}^H\mathbf{H}^{-1}\mathbf{q} + (\lambda - w^*(\infty))\alpha^*\mathbf{A}^H\mathbf{H}^{-1}\mathbf{q}^*. \end{aligned} \tag{65}$$

In analogy to its counterpart before compensation in (12), it is straightforward to obtain the SINR of a GFDM MF receiver over a compensated data block by taking the terms $(1-w^*(\infty)\lambda^*)\alpha$ and $(\lambda - w^*(\infty))\alpha^*$ in the place of α and β respectively in (18); the final expression is given in (66) shown at the bottom of the page.

$$\mathrm{SINR}^{\mathrm{MF}} = \frac{\sum_{n=0}^{N-1}|\mathbf{a}_n^H\mathbf{a}_n|^2}{\sum_{n=0}^{N-1}\sum_{p=0,p\neq n}^{N-1}|\mathbf{a}_n^H\mathbf{a}_p|^2 + \frac{1}{\mathrm{IRR}(\infty)}\sum_{n=0}^{N-1}\sum_{p=0}^{N-1}|\mathbf{a}_n^H\mathbf{b}_p|^2 + \left(1+\frac{1}{\mathrm{IRR}(\infty)}\right)\frac{1}{\mathrm{SNR}}\sum_{n=0}^{N-1}\sum_{p=0}^{N-1}\left|[\mathbf{A}^H\mathbf{H}^{-1}]_{n,p}\right|^2}. \tag{66}$$

In a similar way, for a compensated ZF receiver, we have

$$\begin{aligned}\hat{\mathbf{s}} &= \mathbf{A}^{-1}\mathbf{H}^{-1}(\mathbf{y} - w^*(\infty)\mathbf{y}^*)\\ &= (1 - w^*(\infty)\lambda^*)\alpha\mathbf{s} + (\lambda - w^*(\infty))\alpha^*\mathbf{A}^{-1}\mathbf{H}^{-1}\mathbf{H}^*\mathbf{A}^*\mathbf{s}^*\\ &\quad + (1 - w^*(\infty)\lambda^*)\alpha\mathbf{A}^{-1}\mathbf{H}^{-1}\mathbf{q}\\ &\quad + (\lambda - w^*(\infty))\alpha^*\mathbf{A}^{-1}\mathbf{H}^{-1}\mathbf{q}^*. \end{aligned} \tag{67}$$

and hence, the corresponding SINR is obtained as

$$\mathrm{SINR}^{\mathrm{ZF}} = \frac{N \cdot \mathrm{IRR}(\infty)}{\sum_{n=0}^{N-1}\sum_{p=0}^{N-1} \left|[\mathbf{A}^{-1}\mathbf{B}]_{n,p}\right|^2 + \frac{1+\mathrm{IRR}(\infty)}{\mathrm{SNR}} \sum_{n=0}^{N-1}\sum_{p=0}^{N-1} \left|[\mathbf{A}^{-1}\mathbf{H}^{-1}]_{n,p}\right|^2}. \tag{68}$$

In order to guarantee SINR improvements in GFDM MF and ZF receivers after the proposed NCLMS based I/Q imbalance compensation, by comparing (18) and (23) with (66) and (68) respectively, we need $\mathrm{IRR}(\infty) > 1/|\lambda|^2$. Note that this is also the case which leads to an efficient self-image attenuation by NCLMS, since $1/|\lambda|^2$ is in fact $\mathrm{IRR}(0)$, according to (47). Therefore, based on the analysis in Appendix B, to make this condition valid, the step-size μ must satisfy

$$0 < \mu < \frac{2|\lambda|^2(1 - |\lambda|^2)}{1 + 2|\lambda|^2 - |\lambda|^4}. \tag{69}$$

Remark 6: It is easy to verify that the upper bound on the step-size μ in (69) is a monotonically increasing function of $|\lambda|^2$ for $0 < |\lambda|^2 < \sqrt{2} - 1$. This range covers typical I/Q imbalance situations in receivers, e.g., $|\lambda|^2 \leq 0.0104$ for $|\varepsilon| \leq 0.1$ and $|\theta| \leq 10^\circ$. In other words, the maximum step-size, $\mu_{\max}$, for practical use is roughly 0.02. On the other hand, both the SINR performance of compensated MF and ZF receivers in (66) and (68) are monotonically increasing functions of $\mathrm{IRR}(\infty)$, and hence, monotonically decreasing functions of the step-size, μ, based on (40) and (49). Therefore, these SINR improvements are more pronounced when a smaller step-size μ is employed by NCLMS, and the ideal SINR situation exists only when μ is infinitely small.

VI. Numerical Simulations

In order to verify the analytical performance evaluations of the proposed NCLMS based blind I/Q imbalance compensation for GFDM receivers, computer simulations were conducted based on GFDM transmission systems with $K = 128$ subcarriers and $M = 5$ subsymbols in the data block. A root raised-cosine filter with a roll-off factor at 0.1 was used as the prototype filter of GFDM [3], [4], [37]. The constellation used for symbol mapping was the 16-QAM and the length of CP was 32. A 9-tap static Rayleigh channel was chosen, whose power-delay-profile is given in [6], and white Gaussian noise was added to give a signal-to-noise ratio (SNR) at 20 dB. All the simulation results were obtained by averaging over 1000 independent trials.

We first considered a severely I/Q distorted GFDM receiver with an amplitude mismatch of $\varepsilon = 0.1$ and a phase mismatch of $\theta = 10^\circ$. Fig. 1 shows the theoretical and simulated

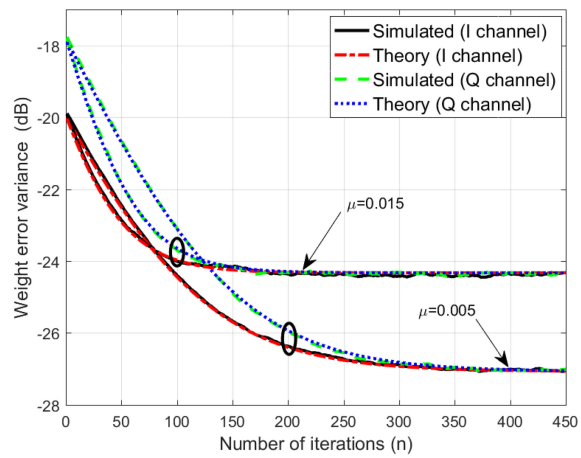

Fig. 1. Comparison of the theoretical and simulated learning curves for the weight error variances in both the I and Q channels, that is, $\varphi_r^2(n)$ and $\varphi_j^2(n)$, of the proposed NCLMS compensator, with step-sizes $\mu = \{0.005, 0.015\}$.

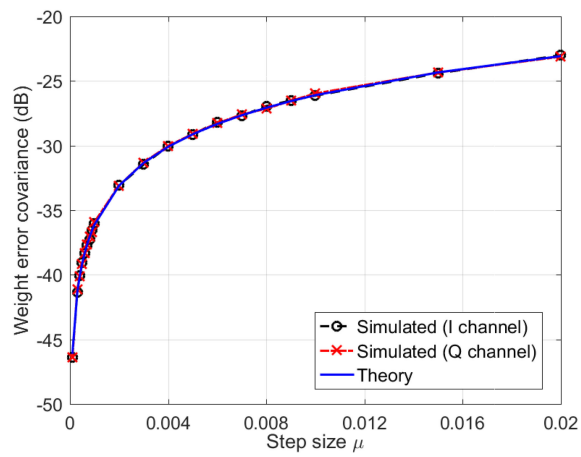

Fig. 2. Steady-state weight error variances in both I and Q channels of the proposed NCLMS compensator, that is, $\varphi_r^2(\infty)$ and $\varphi_j^2(\infty)$, against different step-sizes μ.

convergence behaviors of weight error variances in the I and Q channels, that is, $\varphi_r^2(n)$ and $\varphi_i^2(n)$, within the NCLMS compensator, and the effects of different step-sizes, μ. The theoretical results were obtained by using the proposed full second order performance analysis in (38) and (39) and based on the duality of second order signal statistics between the bivariate real and complex domains in (43). A remarkable agreement was observed between the analytical and simulated results during the entire convergence. The simulation results are in line with *Remark 2*, which states that the improperness of the weight error $\varphi(n)$ is iteratively calibrated during the I/Q imbalance compensation process. This is evidenced by its variance discrepancies (emphasized by the ellipses) in the I and Q channels becoming closer during the convergence. As discussed in *Remark 3*, when NCLMS arrives at its steady-state stage, the weight error $\varphi(\infty)$ becomes purely proper, in theory. As a result, the weight error variances in the I and Q channels, that is, $\varphi_r^2(\infty)$ and $\varphi_j^2(\infty)$, become identical. In other words, both channels make equal contribution to the self-image cancellation capability of the compensator, according to (45) and (49). This analysis is supported by Fig. 2, where the steady states for

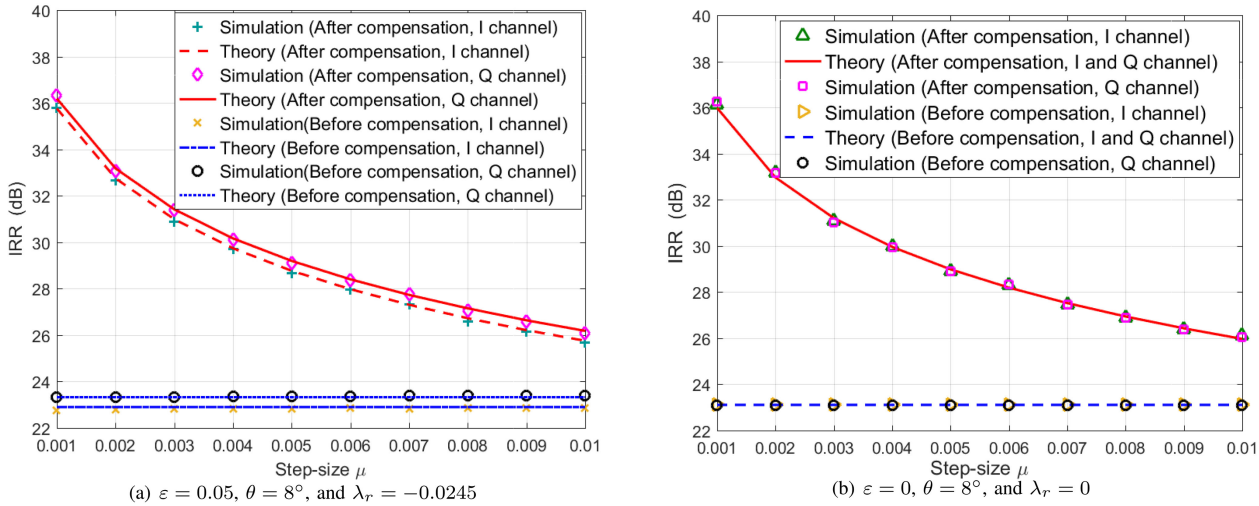

(a) $\varepsilon = 0.05$, $\theta = 8°$, and $\lambda_r = -0.0245$ (b) $\varepsilon = 0$, $\theta = 8°$, and $\lambda_r = 0$

Fig. 3. Comparison of the theoretical and simulated steady-state IRR in both the I and Q channels, that is, $\text{IRR}_I(\infty)$ and $\text{IRR}_Q(\infty)$, of NCLMS with different step-sizes μ. (a) $\lambda_r = -0.0245$, and (b) $\lambda_r = 0$.

TABLE I
COMPARISON OF THEORETICAL AND SIMULATED SINR (DB) OF AN MF RECEIVER BEFORE AND AFTER THE PROPOSED NCLMS BASED I/Q IMBALANCE COMPENSATION, WITH DIFFERENT VALUES OF μ, ε AND θ. THE IDEAL SINR IS 18.57 DB

I/Q mismatches		Before compensation		After compensation							
				μ=0.003		μ=0.001		μ=0.0005		μ=0.0001	
ε	θ	theoretical	simulated	theoretical	simulated	theoretical	simulated	theoretical	simulated	theoretical	simulated
0.1	10°	6.02	6.01	12.95	12.92	15.84	15.80	16.98	16.95	18.21	18.19
0.08	8°	7.71	7.68	12.96	12.95	15.83	15.82	16.99	16.97	18.22	18.19
0.06	−6°	9.94	9.97	12.97	12.96	15.85	15.82	16.99	16.95	18.23	18.20
0.05	5°	11.27	11.24	12.96	12.94	15.83	15.81	17.01	16.99	18.21	18.18

the I and Q channels, $\varphi_r^2(\infty)$ and $\varphi_j^2(\infty)$, are plotted against different step-sizes, μ, from 0.0001 to 0.02. The close match between the analytical and empirical results was observed.

The proposed full second order performance analysis also enables us to decouple and subsequently to quantify the impacts of self-image interference introduced by amplitude and phase mismatches on the I and Q channels, both before and after the proposed compensation. This is demonstrated in Fig. 3(a), where the steady-state IRRs of both the I and Q channels, that is, $\text{IRR}_I(\infty)$ and $\text{IRR}_Q(\infty)$, achieved by NCLMS and evaluated by (63) and (64), were compared with their simulated counterparts for different step-sizes μ. Their initializations $\text{IRR}_I(0)$ and $\text{IRR}_Q(0)$, calculated by (55), are also provided, serving as benchmarks. The considered I/Q imbalanced GFDM receiver was with $\varepsilon = 0.05$, $\theta = 8°$, and consequently, $\lambda_r = -0.0245$. The simulations in Fig. 3(a) conform with our analysis in *Remark 5* which states that between the I and Q channels, the difference of the power ratio between the desired signal and its image interference component does exist, no matter before or after the compensation. This physical property of I/Q imbalanced receivers is introduced by a nonzero λ_r, and hence, vanishes only when $\lambda_r = 0$, as shown in Fig. 3(b). Both Fig. 3(a) and Fig. 3(b) validate our proposed IRR evaluations in both the I and Q channels and against different step-sizes; we also observe that NCLMS achieved enhanced image attenuations in both the I and Q channels, especially when a smaller step-size μ was employed, although at a cost in convergence properties.

In the next stage, the self-image attenuation capability of the NCLMS compensator was further evaluated in terms of SINR of GFDM receivers. Theoretically, due to insufficient degrees of freedom, blind methods cannot decouple the channel effects from the exact I/Q imbalance amount of the receiver. Therefore, in this experiment, perfect channel information was assumed to be known. Table I and Table II illustrate that considerable SINR improvements in both MF and ZF receivers were achieved by NCLMS, especially with a small step-size μ. Those improvements were robust over different I/Q mismatches, while due to the underlying physics, ZF receivers inherently had better immunity to self-interference than their MF counterparts for identical I/Q imbalance situations. Again, the theoretical SINR evaluation of both MF and ZF receivers by using (66) and (68) accurately described their simulated SINRs in different I/Q imbalance scenarios.

In the last set of simulations, we investigated the robustness of the proposed I/Q imbalance compensator when integrated with GFDM receivers in terms of uncoded bit error rate (BER). The simulated MF and ZF receivers were contaminated by identical I/Q mismatches with $\varepsilon = 0.1$ and $\theta = -8°$. Their compensated and equalized GFDM data were respectively obtained by using (65) and (67), and were further used for the BER evaluation. The BER results of both receivers before and after the proposed compensation are plotted in Fig. 4(a) and (b) as functions of the SNR and the step-size μ. Several interesting phenomena can be observed from Fig. 4(a). First, before

TABLE II
COMPARISON OF THEORETICAL AND SIMULATED SINR (dB) OF A ZF RECEIVER BEFORE AND AFTER THE PROPOSED NCLMS BASED I/Q IMBALANCE COMPENSATION, WITH DIFFERENT VALUES OF μ, ε AND θ. THE IDEAL SINR IS 30.01 dB

I/Q mismatches		Before compensation		After compensation							
				μ=0.003		μ=0.001		μ=0.0005		μ=0.0001	
ε	θ	theoretical	simulated	theoretical	simulated	theoretical	simulated	theoretical	simulated	theoretical	simulated
0.1	10°	6.38	6.34	14.44	14.41	19.07	19.04	21.99	21.96	26.76	26.73
0.08	−5°	11.01	10.96	14.42	14.39	19.05	19.01	21.98	21.97	26.77	26.75
0.05	8°	8.93	8.91	14.43	14.38	19.05	19.04	22.00	21.95	26.78	26.73
0.05	5°	12.31	12.30	14.42	14.40	19.06	19.03	21.98	21.96	26.76	26.74

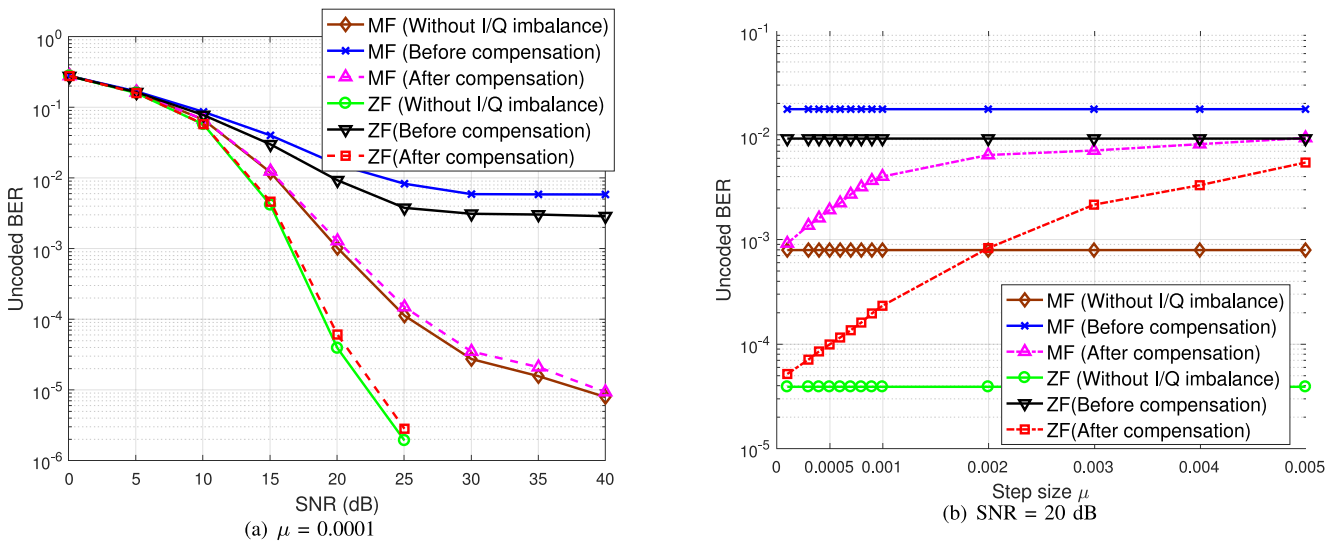

(a) μ = 0.0001 (b) SNR = 20 dB

Fig. 4. BER performance of MF and ZF receivers before and after I/Q imbalance compensation against (a) different SNRs and (b) different step-sizes μ.

the compensation, unlike the ideal situation, the I/Q imbalance made no obvious BER difference between MF and ZF receivers. Second, their BERs became nearly saturated in the high SNR region, e.g., SNR > 25 dB, so that even increasing the operating SNR did not bring obvious performance improvements. This is because the self-interference introduced by I/Q imbalance was dominant, as compared with the additive channel noise. On the other hand, after applying the proposed NCLMS based I/Q imbalance compensator, the immunities of MF and ZF receivers to bit error were greatly improved. As expected, a smaller step-size μ enabled the proposed compensator a more accurate data recovery in both MF and ZF receivers, as demonstrated by Fig. 4(b).

VII. CONCLUSION

In order to alleviate the performance deterioration introduced by I/Q imbalance on generalized frequency division multiplexing (GFDM) direct-conversion receivers, a normalized complex least mean square (NCLMS) based blind compensator has been proposed, together with a novel full second order performance analysis, established by investigating the evolutions of the weight error covariance and complementary covariance in both the transient and steady-state stages. In this way, we have conducted an accurate evaluation of its excellent self-image attenuation capability via a rigorous image rejection ratio (IRR) analysis, and have provided intrinsic physical insights underlying the proposed NCLMS compensator. We have also shown that, as a byproduct of its adaptive I/Q imbalance compensation process, the weight error coefficient becomes purely proper in theory. An important finding is that, after the compensation, the I and Q channels contribute equally to the overall self-image attenuation performance, although the individual IRR situations along I and Q channels are in general different. In addition, the proposed full second order performance analysis has facilitated closed-form relationships between the improvements in both IRR and signal-to-interference plus noise ratio (SINR) by NCLMS and its step-size for GFDM matched filter (MF) and zero forcing (ZF) receivers. Simulations using GFDM waveforms support the analysis.

APPENDIX A
DETAILED DERIVATION OF $\lambda_r = 0$

According to the definition of the imbalance coefficient λ,

$$\lambda \triangleq \frac{\beta}{\alpha^*} = \frac{\beta_r + j\beta_j}{\alpha_r - j\alpha_j} = \frac{\alpha_r\beta_r - \alpha_j\beta_j + j(\alpha_j\beta_r + \alpha_r\beta_j)}{\alpha_r^2 + \alpha_j^2}, \tag{70}$$

where,

$$\lambda_r = \frac{\alpha_r \beta_r - \alpha_j \beta_j}{\alpha_r^2 + \alpha_j^2}. \tag{71}$$

Based on (6) and (7), we obtain

$$\alpha_r = \frac{1 + (1+\varepsilon)\cos(\theta)}{2}, \tag{72}$$

$$\beta_r = \frac{1 - (1+\varepsilon)\cos(\theta)}{2}, \tag{73}$$

$$\alpha_j = \beta_j = -\frac{(1+\varepsilon)\sin(\theta)}{2}. \tag{74}$$

A substitution of (72), (73) and (74) into (71) yields

$$\lambda_r = \frac{1 - (1+\varepsilon)^2}{1 + (1+\varepsilon)^2 + 2(1+\varepsilon)\cos(\theta)}. \tag{75}$$

It is then straightforward to see that $\lambda_r = 0$ occurs when the amplitude mismatch $\varepsilon = 0$ or $\varepsilon = -2$, however, the latter is not physically reasonable for practical I/Q imbalance modeling.

Appendix B
Bound on the Step-Size μ for An Efficient I/Q Imbalance Compensation

In order to achieve $\text{IRR}(\infty) > 1/|\lambda|^2$, based on (49), we have

$$\frac{(1-|\lambda|^2)^2}{\kappa(\infty)} + |\lambda|^2 > \frac{1}{|\lambda|^2}, \tag{76}$$

and after a few mathematical manipulations, this is equivalent to considering

$$\kappa(\infty) < \frac{|\lambda|^2(1-|\lambda|^2)}{1+|\lambda|^2}. \tag{77}$$

Now, a substitution of (40) into (77) yields (69).

References

[1] N. Michailow *et al.*, "Generalized frequency division multiplexing for 5th generation cellular networks," *IEEE Trans. Commun.*, vol. 62, no. 9, pp. 3045–3061, Sep. 2014.

[2] B. Farhang-Boroujeny and H. Moradi, "OFDM inspired waveforms for 5G," *IEEE Commun. Surv. Tut.*, vol. 18, no. 4, pp. 2474–2492, Fourth Quarter 2016.

[3] N. Michailow, I. Gaspar, S. Krone, M. Lentmaier, and G. Fettweis, "Generalized frequency division multiplexing: Analysis of an alternative multicarrier technique for next generation cellular systems," in *Proc. Int. Symp. Wireless Commun. Syst.*, Aug. 2012, pp. 171–175.

[4] A. Kumar, M. Magarini, and S. Bregni, "Impact of "Better than Nyquist" pulse shaping in GFDM PHY with LTE-compatible frame structure," in *Proc. IEEE Latin-Amer. Conf. Commun.*, Nov. 2017, pp. 1–4.

[5] I. Gaspar, N. Michailow, A. Navarro, E. Ohlmer, S. Krone, and G. Fettweis, "Low complexity GFDM receiver based on sparse frequency domain processing," in *Proc. IEEE Int. Conf. Veh Technol.*, Jun. 2013, pp. 1–6.

[6] P. Wei, X.-G. Xia, Y. Xiao, and S. Li, "Fast DGT-based receivers for GFDM in broadband channels," *IEEE Trans. Commun.*, vol. 64, no. 10, pp. 4331–4315, Oct. 2016.

[7] P.-C. Chen, B. Su, and Y. Huang, "Matrix characterization for GFDM: Low complexity MMSE receivers and optimal filters," *IEEE Trans. Signal Process.*, vol. 65, no. 18, pp. 4940–4955, Sep. 2017.

[8] S. Han, Y. Sung, and Y. H. Lee, "Filter design for generalized frequency division multiplexing," *IEEE Trans. Signal Process.*, vol. 65, no. 7, pp. 1644–1659, Apr. 2017.

[9] M. Matthé, L. L. Mendes, N. Michailow, D. Zhang, and G. Fettweis, "Widely linear estimation for space-time-coded GFDM in low-latency applications," *IEEE Trans. Commun.*, vol. 63, no. 11, pp. 4501–4509, Nov. 2015.

[10] D. Zhang, L. L. Mendes, M. Matthé, I. S. Gaspar, N. Michailow, and G. P. Fettweis, "Expectation propagation for near-optimum detection of MIMO-GFDM signals," *IEEE Trans. Wireless Commun.*, vol. 15, no. 2, pp. 1045–1062, Feb. 2016.

[11] S. Mirabbasi and K. Martin, "Classical and modern receiver architectures," *IEEE Commun. Mag.*, vol. 38, no. 11, pp. 132–139, Nov. 2000.

[12] Y. C. Pan and S. M. Phoong, "A time-domain joint estimation algorithm for CFO and I/Q imbalance in wideband direct-conversion receivers," *IEEE Trans. Wireless Commun.*, vol. 11, no. 7, pp. 2353–2361, Mar. 2012.

[13] G. T. Gil, I. H. Sohn, J. K. Park, and Y. H. Lee, "Joint ML estimation of carrier frequency, channel, I/Q mismatch, and DC offset in communication receivers," *IEEE Trans. Veh. Technol.*, vol. 54, no. 1, pp. 338–349, Jan. 2005.

[14] M. Marey, M. Samir, and M. H. Ahmed, "Joint estimation of transmitter and receiver IQ imbalance with ML detection for Alamouti OFDM systems," *IEEE Trans. Veh. Technol.*, vol. 62, no. 6, pp. 2847–2853, Jul. 2013.

[15] F. Horlin, A. Bourdoux, and L. V. D. Perre, "Low-complexity EM-based joint acquisition of the carrier frequency offset and IQ imbalance," *IEEE Trans. Wireless Commun.*, vol. 7, no. 6, pp. 2212–2220, Jun. 2008.

[16] A. Tarighat, R. Bagheri, and A. H. Sayed, "Compensation schemes and performance analysis of IQ imbalances in OFDM receivers," *IEEE Trans. Signal Process.*, vol. 53, no. 8, pp. 3257–3268, Aug. 2005.

[17] K. Sun and C. Chao, "Estimation and compensation of I/Q imbalance in OFDM direct-conversion receivers," *IEEE J. Sel. Topics Signal Process.*, vol. 3, no. 3, pp. 438–453, Jun. 2009.

[18] A. Hakkarainen, J. Werner, K. R. Dandekar, and M. Valkama, "Widely-linear beamforming and RF impairment suppression in massive antenna arrays," *J. Commun. Netw.*, vol. 15, no. 4, pp. 383–397, Aug. 2013.

[19] Z. Li, Y. Xia, W. Pei, K. Wang, Y. Huang, and D. P. Mandic, "Noncircular measurement and mitigation of I/Q imbalance for OFDM-based WLAN transmitters," *IEEE Trans. Instrum. Meas.*, vol. 66, no. 3, pp. 383–393, Mar. 2017.

[20] J. J. Witt and G. J. Rooyen, "A blind I/Q imbalance compensation technique for direct-conversion digital radio transceivers," *IEEE Trans. Veh. Technol.*, vol. 58, no. 4, pp. 2077–2082, May 2009.

[21] M. Valkama, M. Renfors, and V. Koivunen, "Blind signal estimation in conjugate signal models with application to I/Q imbalance compensation," *IEEE Signal Process. Lett.*, vol. 12, no. 11, pp. 733–736, Nov. 2005.

[22] G. T. Gil, "Normalized LMS adaptive cancellation of self-image in direct-conversion receivers," *IEEE Trans. Veh. Technol.*, vol. 58, no. 2, pp. 535–545, Feb. 2009.

[23] L. Anttila, M. Valkama, and M. Renfors, "Circularity-based I/Q imbalance compensation in wideband direct-conversion receivers," *IEEE Trans. Veh. Technol.*, vol. 57, no. 4, pp. 2099–2113, Jul. 2008.

[24] L. Anttila and M. Valkama, "Blind signal estimation in widely-linear signal models with fourth-order circularity: Algorithms and application to receiver I/Q calibration," *IEEE Signal Process. Lett.*, vol. 20, no. 3, pp. 221–224, Mar. 2013.

[25] Y. Tsai, C.-P. Yen, and X. Wang, "Blind frequency-dependent I/Q imbalance compensation for direct-conversion receivers," *IEEE Trans. Wireless Commun.*, vol. 9, no. 6, pp. 1976–1986, Jun. 2010.

[26] W. Nam, H. Roh, J. Lee, and I. Kang, "Blind adaptive I/Q imbalance compensation algorithms for direct-conversion receivers," *IEEE Signal Process. Lett.*, vol. 19, no. 8, pp. 475–478, Aug. 2012.

[27] F. D. Neeser and J. L. Massey, "Proper complex random processes with applications to information theory," *IEEE Trans. Inf. Theory*, vol. 39, no. 4, pp. 1293–1302, Jul. 1993.

[28] B. Picinbono, "On circularity," *IEEE Trans. Signal Process.*, vol. 42, no. 12, pp. 3473–3482, Dec. 1994.

[29] B. Picinbono and P. Chevalier, "Widely linear estimation with complex data," *IEEE Trans. Signal Process.*, vol. 43, no. 8, pp. 2030–2033, Aug. 1995.

[30] D. P. Mandic and S. L. Goh, *Complex Valued Nonlinear Adaptive Filters: Noncircularity, Widely Linear and Neural Models*. New York, NY, USA: Wiley, 2009.

[31] P. J. Schreier and L. L. Scharf, *Statistical Signal Processing of Complex-Valued Data: The Theory of Improper and Noncircular Signals*. Cambridge, U.K.: Cambridge Univ. Press, 2010.

[32] M. Lupupa and J. Qi, "I/Q imbalance in generalized frequency division multiplexing under Weibull fading," in *Proc. IEEE Int. Symp. Personal Indoor Mobile Radio Commun.*, Sep. 2015, pp. 471–476.

[33] N. Tang, S. He, C. Xue, Y. Huang, and L. Yang, "IQ imbalance compensation for generalized frequency division multiplexing systems," *IEEE Wireless Commun. Lett.*, vol. 6, no. 4, pp. 422–425, Apr. 2017.
[34] Y. Xia and D. P. Mandic, "Complementary mean square analysis of augmented CLMS for second order noncircular Gaussian signals," *IEEE Signal Process. Lett.*, vol. 24, no. 9, pp. 1413–1417, Sep. 2017.
[35] Y. Xia and D. P. Mandic, "A full mean square analysis of CLMS for second order noncircular inputs," *IEEE Trans. Signal Process.*, vol. 65, no. 21, pp. 5578–5590, Nov. 2017.
[36] Y. Xia and D. P. Mandic, "Augmented performance bounds on strictly linear and widely linear estimators with complex data," *IEEE Trans. Signal Process.*, vol. 66, no. 2, pp. 507–514, Jan. 2018.
[37] B. Lim and Y. C. Ko, "SIR analysis of OFDM and GFDM waveforms with timing offset, CFO and phase noise," *IEEE Trans. Wireless Commun.*, vol. 16, no. 10, pp. 6979–6990, Oct. 2017.
[38] S. Tiwari, D. S. Sekhar, and K. K. Bandyopadhyay, "Precoded generalised frequency division multiplexing system to combat inter-carrier interference: Performance analysis," *IET Commun.*, vol. 9, no. 15, pp. 1829–1841, May 2015.
[39] N. Michailow, S. Krone, M. Lentmaier, and G. Fettweis, "Bit error rate performance of generalized frequency division multiplexing," in *Proc. IEEE Int. Conf. Veh. Technol.*, Sep. 2012, pp. 1–5.
[40] K. A. Hamdi, "Exact SINR analysis of wireless OFDM in the presence of carrier frequency offset," *IEEE Trans. Wireless Commun.*, vol. 9, no. 3, pp. 975–979, Mar. 2010.
[41] B. Widrow and S. D. Stearns, *Adaptive Signal Processing*. Englewood Cliffs, NJ, USA: Prentice-Hall, 1985.
[42] A. Gersho, "Adaptive equalization of highly dispersive channels for data transmission," *Bell Syst. Tech. J.*, vol. 48, pp. 55–70, Jan. 1969.
[43] G. Underboeck, "Theory on the speed of convergence in adaptive equalizers for digital communication," *IBM J. Res. Develop.*, vol. 16, pp. 546–555, Nov. 1972.
[44] M. Valkama, M. Renfors, and V. Koivunen, "On the performance of interference canceller based I/Q imbalance compensation," in *Proc. IEEE Int. Conf. Acoust. Speech Signal Process.*, Jun. 2000, pp. 2885–2888.
[45] S. Wei, D. L. Goechel, and P. A. Kelly, "Convergence of the complex envelope of bandlimited OFDM signals," *IEEE Trans. Inf. Theory*, vol. 56, no. 10, pp. 4893–4904, Oct. 2010.
[46] D. Tse and P. Viswanath, *Fundamentals of Wireless Communications*. Cambridge, U.K.: Cambridge Univ. Press, 2005.
[47] Y. Yoshida, K. Hayashi, H. Sakai, and W. Bocquet, "Analysis and compensation of transmitter IQ imbalances in OFDMA and SC-FDMA systems," *IEEE Trans. Signal Process.*, vol. 57, no. 8, pp. 3119–3129, Aug. 2009.

Hao Cheng (S'18) received the B.S. degree in electronic information engineering from Yangzhou University, Yangzhou, China, in 2011, and the M.S. degree in signal and information processing from the Nanjing University of Aeronautics and Astronautics, Nanjing, China, in 2014. He is currently working toward the Ph.D. degree at the School of Information Science and Engineering, Southeast University, Nanjing, China.

His current research interests include air interface waveform design, adaptive filters, and Internet of things.

Yili Xia (M'11) received the B.Eng. degree in information engineering from Southeast University, Nanjing, China, in 2006, and the M.Sc. (with distinction) degree in communications and signal processing from the Department of Electrical and Electronic Engineering, in 2007 and the Ph.D. degree in adaptive signal processing both from Imperial College London, London, U.K. in 2011.

Since 2013, he has been an Associate Professor with the School of Information and Engineering, Southeast University, Nanjing, China, where he is currently the Deputy Head of the Department of Information and Signal Processing Engineering. His research interests include complex and hyper-complex statistical analysis, linear and nonlinear adaptive filters, as well as their applications on communications and power systems.

Yongming Huang (M'10–SM'16) received the B.S. and M.S. degrees from Nanjing University, Nanjing, China, in 2000 and 2003, respectively, and the Ph.D. degree in electrical engineering from Southeast University, Nanjing, China, in 2007.

Since 2007, he has been a Faculty Member with the School of Information Science and Engineering, Southeast University, where he is currently a Full Professor. From 2008 to 2009, he visited the Signal Processing Laboratory, School of Electrical Engineering, Royal Institute of Technology, Stockholm, Sweden. He has authored more than 200 peer-reviewed papers, submitted more than ten technical contributions to the IEEE standards, and hold more than 50 invention patents. His current research interests include MIMO wireless communication, cooperative wireless communication, and millimeter wave wireless communication. He was an Associate Editor for the IEEE TRANSACTIONS ON SIGNAL PROCESSING, the IEEE Wireless Communications Letters, *EURASIP Journal on Advances in Signal Processing*, and *EURASIP Journal on Wireless Communications and Networking*.

Luxi Yang (M'96) received the M.S. and Ph.D. degrees in electrical engineering from the Southeast University, Nanjing, China, in 1990 and 1993, respectively.

Since 1993, he has been with the Department of Radio Engineering, Southeast University, where he is currently a Full Professor of information systems and communications, and the Director of Digital Signal Processing Division. His current research interests include signal processing for wireless communications, MIMO communications, cooperative relaying systems, and statistical signal processing. He has authored or coauthored of two published books and more than 100 journal papers, and holds 30 patents. He was the recipient of the first and second class prizes of science and technology progress awards of the state education ministry of China in 1998, 2002, and 2014. He is currently a member of Signal Processing Committee of Chinese Institute of Electronics.

Danilo P. Mandic (M'99–SM'03–F'12) received the Ph.D. degree in nonlinear adaptive signal processing in 1999 from Imperial College London, London, U.K.

He is currently a Professor in signal processing. He has been working in the area of nonlinear adaptive signal processing, multivariate data analysis, and nonlinear dynamics. He has been a Guest Professor with Katholieke Universiteit Leuven, Leuven, Belgium, the Tokyo University of Agriculture and Technology, Tokyo, Japan, and Westminster University, London, and a Frontier Researcher with RIKEN, Japan. His publications include two research monographs entitled *Recurrent Neural Networks for Prediction*: *Learning Algorithms*, *Architectures and Stability* (1st ed., Wiley, Aug. 2001) and *Complex Valued Nonlinear Adaptive Filters*: *Noncircularity*, *Widely Linear and Neural Models* (1st ed., Wiley, Apr. 2009), an edited book titled *Signal Processing Techniques for Knowledge Extraction and Information Fusion* (Springer, 2008), and more than 200 publications on signal and image processing.

Prof. Mandic has been a member of the IEEE Technical Committee on Signal Processing Theory and Methods, and has been an Associate Editor for the IEEE TRANSACTIONS ON CIRCUITS AND SYSTEMS II, the IEEE TRANSACTIONS ON SIGNAL PROCESSING, the IEEE TRANSACTIONS ON NEURAL NETWORKS, and the *International Journal of Mathematical Modelling and Algorithms*. He is currently an Associate Editor for the IEEE SIGNAL PROCESSING MAGAZINE, and the IEEE TRANSACTIONS ON INFORMATION AND SIGNAL PROCESSING OVER NETWORKS. He has produced award winning papers and products resulting from his collaboration with Industry.